# Evaluation of structures affected by Alkali-Silica reaction (ASR) using homogenized modelling of reinforced concrete

Daniela Vo, Stéphane Multon, Pierre Morenon, Alain Sellier, Etienne Grimal, Benoit Masson, Philippe Kolmayer

# Evaluation of structures affected by Alkali-Silica Reaction (ASR) using homogenized modelling of reinforced concrete

Daniela Vo[0,1], Stéphane Multon[1], Pierre Morenon[1,2], Alain Sellier[1], Etienne Grimal[3], Benoit Masson[4], Philippe Kolmayer[3]

[0]Corresponding author: daniela.vo@outlook.com

[1]LMDC, Université de Toulouse III – Paul Sabatier, F-31077 Toulouse Cedex 04, France

[2] Toulouse Tech Transfer, 118 route de Narbonne, CS 24246, 31432 Toulouse Cedex 04, France

[3]EDF-CIH Technolac, 73373 Le Bourget du Lac, Cedex, France

[4]EDF-DIPNN, 69007 Lyon, France

## Abstract

The computation of large reinforced concrete structures such as nuclear power plants, dams and bridges requires realistic behaviour laws to be considered for concrete and reinforcements. ~~The classical way to do this is to use finite element methods in which rebars and concrete are meshed separately.~~ Regarding the problem of cracking in RC structure, meshing separately concrete and rebars is the classical way to perform a nonlinear finite element analysis. However, when the structures have to be studied at full scale, the explicit meshing of rebars becomes so heavy that the computing time reaches values incompatible with engineering applications. The method proposed in this paper consists of using large finite elements considering reinforcement and concrete as a homogenized material. In comparison to the mesh reinforcement approach, this one ~~This~~ limits the number of finite elements and returns to a computation compatible with engineering. The particularity of the proposed model resides in its ability to treat interaction between rebars and concrete affected by the Alkali-Silica Reaction (ASR). The model is able to predict the anisotropic swelling induced by the combination of homogenized rebars and external loadings. An application to a well-documented laboratory test for reinforced concrete beams shows the ability of the model to assess residual strength capacity of the beam after a long period of ageing in a natural environment. A parametric study of the size of the finite elements confirms the possibility of using a coarse mesh without loss of the model's predictive capability.

Keywords: Alkali-Silica Reaction, reinforced concrete, finite element

## 1. Introduction

Alkali-Silica Reaction (ASR) is an endogenous chemical reaction that damages concrete. It can induce structural damage as it alters the mechanical strengths of the material. Although the exact reaction mechanisms are still under discussion in the literature, the main ones have been identified [1] [2] [3]. Through various combined chemical reactions, the alkalis of the pore solution react with the silica present in amorphous or slightly crystallized phases contained in aggregates, first attacked by hydroxyl ions. This reaction leads to the production of new phases in the porosity and to swelling of the concrete. From the mechanical point of view, the action of ASR in concrete can be represented by an internal pressure. When the stress resulting from this pressure exceeds the local tensile strength, irreversible cracking is induced. Stresses on the matrix from other sources also play a major role in expansion as the stress state leads to the development of preferential directions for induced expansions and, hence, for cracks and damage [4] [5] [6] [7] [8] [9] [10]. Such ASR damage modifies the bearing capacity of the affected structures and modelling is necessary to evaluate the structural safety. The characterization of ASR-damage and the modelling of its impact can also be used to optimize and facilitate repairs and rehabilitation works.

Constitutive models are generally established after experimental and laboratory studies and may be validated by confrontation with results obtained on laboratory structures. Hence, the use of such models for real damaged structures may be questionable due to the differences between ASR mechanisms in laboratory conditions and in the actual environment of the structure concerned. Due to the difference between ASR scale and structural scale, the establishment of multi-scale approaches constitutes a topical and a complex issue. These last years, efforts have been done towards the multi-scale model development [11] [12] [13]. Hence, different approaches can be found in the literature. According to [14], they can be distinguished in different categories: models based on concrete expansion, models based on internal pressure, models based on gel production and model based on ions diffusion reaction Note that in this paper, the ASR modelling belongs to the category of gel production types. Further complexity may be introduced if the structures are highly reinforced. Reinforcements in ASR-affected structures cause restrained expansion, chemical prestressing and oriented cracking. For numerical simulations, this can lead to several difficulties. ASR expansion restrained by the reinforcement steel leads to the development of stress concentration in the steel-concrete interface zone. For modelling based on damage theory, such stress localized in small zones of the mesh can induce an overestimation of the damage and a total loss of bonding between the concrete and the reinforcement bar. However, recent experimental work [15] indicates that this modelled phenomenon may not be realistic. Because of this unrealistic evaluation of stress at the interface between concrete and steel, the whole mechanical behaviour of the structure is misrepresented. In order to avoid such numerical complexities, and limit computational times, reinforcement can be modelled by assuming reinforced concrete to be a single material containing concrete and rebars, where the reinforcement bars do not have to be specifically meshed [16] [17] [18]. The steel contribution is evaluated along the directions of reinforcements through their own behavioural laws. The reinforced concrete response is then assessed by a mixing law combining steel and concrete contributions, according to the concrete/steel ratio. From the application point of view, and comparatively with approach needing the meshing of the reinforcements, such a homogenization approach can lead to significant time saving, particularly for highly reinforced structures. As reinforcement does not have to be explicitly meshed, the structures can be evaluated with large sized elements, thus reducing computation times without significant loss of prediction capability.

The aim of this paper is to validate the suitability of combining ASR-modelling with the assumption of homogenized reinforcement, by comparing model predictions with experimental results from the literature. This comparison is performed for the two main phases of the service life of the structures: the ageing period (development of expansion) and the final bending, so as to assess the capacity of the model to represent both the Service Limit State (SLS) and the Ultimate Limit State (ULS) of the structure. It is also important to verify the dependence of the model on the mesh size in such modelling. This is the second objective of this paper. It is attained through a parametrical study on the sizes of the finite elements.

The main features of the model used in this work are presented first. Then the model is validated through a comparison with the experimental works performed by Ohno et al. [19] on the mechanical behaviour of beams affected by ASR. During the period of aging, the beams were subjected to natural weather, with small moisture gradients, to allow ASR advancement to develop without laboratory acceleration. After this, they were subjected to a four-point bending test until failure. Due to the induced chemical prestressing, the strain during the ageing phase and the flexural response of reactive beams were different from those of non-reactive beams. Strain evolution during the ageing period is analysed, as are the load/displacement curves and the crack patterns obtained during the simulation of the bending test. The sensitivity of the model to the mesh size is discussed for the two periods.

## 2. Constitutive model

In the present study, the reinforced concrete structure is modelled through a homogenized approach in which the reinforced concrete matrix is considered as a single material. The contributions of the concrete and the steel reinforcement are evaluated separately before being combined in a ~~homogenized law~~ single behaviour law according to their relative quantities. ~~The global mechanical scheme combining concrete and steel modelling is presented in(~~ Figure 1)

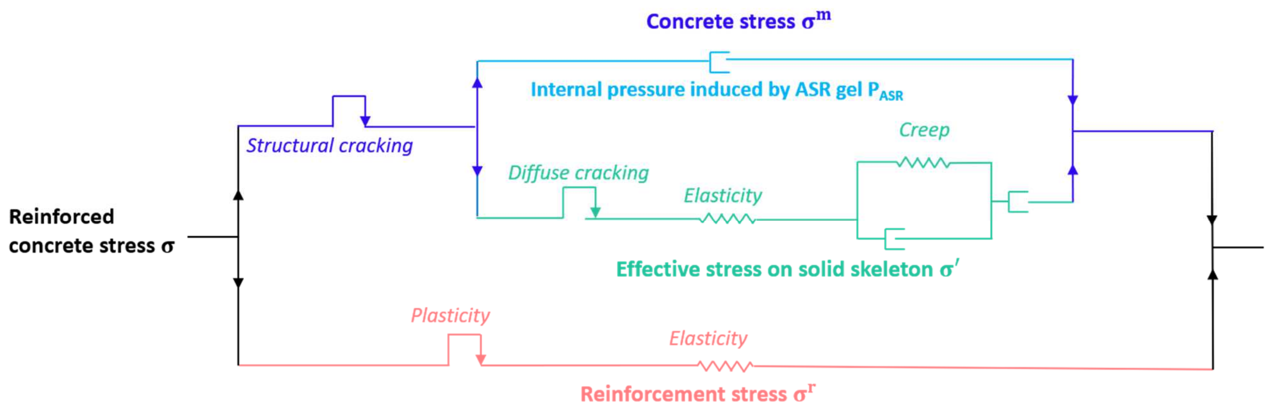


*Figure 1: Rheological scheme: concrete and reinforcement modelling combined in a single reinforced concrete behaviour law*

The different terms defined in Figure 1 are combined by a global Equation (17) which will be presented after the definition of each term. In the first section, the ASR pressure and damage are presented and in the following some aspects of concrete and reinforcement behaviours are specified.

To model the internal expansion induced ~~by ASR~~, the poromechanical framework presented in [20] and [21] is used. This theory allows the solid phases of the matrix to be differentiated from the interstitial ones. The concrete stress $\sigma^m$ is split in two parts: the internal pressure $P_{ASR}$ due to the new phases produced by ASR, and the effective stress $\sigma'$ applied to the solid skeleton of the concrete matrix (Figure 1).

Considering the reduction of mechanical properties due to ASR or external loading, the model is also defined according to the damage theory of [22]. In this framework, the effective stress is defined with respect to the ~~healthy~~ sound part of the concrete. Hence, the effective stress in the damage sense is the concrete stress $\sigma^m$. Therefore, the total induced stress is the mean stress on the total surface of the material. The relation between effective and total stress is obtained from the evaluation of damage.

In concrete structures, the cracks due to external loading or to strain gradients are localized. They are called 'structural cracking' in this paper. For ASR-affected structures, such structural cracks can ~~must~~ be distinguished from material cracks due to internal expansion caused by ASR at the aggregate scale: The formulation of the model distinguishes the two types of cracking with two types of criteria.

Structural cracks are induced by the "total" principal stresses, while the diffuse cracking due to ASR starts in the reactive aggregates. The stress induced by the gel pressure can be possibly balanced by macroscopic compressive stress (which induces anisotropic cracking and then anisotropic swelling). Material cracking due to ASR is called 'diffuse cracking' here, as in Figure 1. In the present model, the distinction between the two types of cracking is made by two different criteria. At macroscopic scale, a smeared crack approach [23] is used to manage the structural cracking.~~ For the structural cracking at macroscopic scale, c~~ Compressive and shear effects are managed by a non-associated Drucker-Prager criterion that controls the evolution of the corresponding plastic strains. Tensile macroscopic effects are driven by three associated orthogonal Rankine criteria (in the main directions of tension). For the diffuse cracking, a same kind of Rankine criteria are used but written in terms of the main poromechanical effective stresses.

Once ASR cracking is initiated, it reduces the mechanical characteristics. Different damage variables are used in the model (according to external/internal phenomena). As this paper focuses on assessing reinforced concrete structures damaged by ASR, only some aspects of the model are presented here. All the other aspects of the model can be found in [16].

## 2.1. Alkali-Silica Reaction

### 2.1.1. Advancement

To model the ASR induced swelling, the advancement must first be assessed. More than cut-off limits for the reaction to take place, the environmental conditions strongly impact the evolution of its kinetics. Hence advancement evaluation must take them into account. Note that, in the present work, the variation of the saturation degree in the concrete is assumed to be negligible.

Thus, ASR advancement degree $A^{ASR}$ is defined by the following equation, based on Poyet's work [24] [25]:

$$\frac{\partial A^{ASR}}{\partial t} = \frac{1}{\tau_{ref}^{ASR}} C^{T,ASR} \cdot \cancel{\left(1 - A^{ASR}\right)_+} \left(1 - A^{ASR}\right) \qquad (1)$$

where $\tau_{ref}^{ASR}$ is a material parameter driving the ASR kinetics, calibrated at the absolute reference temperature $T_{ref}$. $\cancel{C^{T,RAG}}C^{T,ASR}$ is the coefficient that modifies the kinetics according to the temperature.

Larive [26] highlighted the non-linear impact of temperature on ASR-kinetics. It can be characterized by an Arrhenius law, with an activation energy, $E^{ASR}$ , estimated at 40 kJ/mol:

$$C^{T,ASR} = exp\left(-\frac{E^{ASR}}{R}\left(\frac{1}{T}-\frac{1}{T_{ref}}\right)\right) \tag{2}$$

### 2.1.2. Effective gel of ASR

In most of experimental studies, ASR expansion evolves according to three phases: a latency period, an acceleration of the expansion and, finally, a strain plateau. Several mechanisms can explain the latency period. Physical considerations include the time necessary for ASR phases to induce sufficient pressure to cause internal cracks [27] [28]. Chemical considerations can also explain the latency period by the succession of chemical reactions according to the chemical equilibrium in the pore solution [3]. Whatever the reason, poromechanical modelling has to be able to reproduce this latency time during which chemical reaction starts without inducing expansion. It can be considered through the notion of effective volume of gel:

- As long as the advancement is lower than a threshold, the phases produced by ASR do not induce effective expansion,
- Once this advancement threshold is reached, the expansion begins.

It can be obtained by the following equations:

$$\begin{aligned} \Phi_{ASR}^{eff} &= \Phi^{ASR,\infty}\frac{(A(t)-A_{LAT})}{(1-A_{LAT})} \quad if\ A(t) > A_{LAT} \\ \Phi_{ASR}^{eff} &= 0 \qquad\qquad\qquad\qquad if\ A(t) < A_{LAT} \end{aligned} \tag{3}$$

with $\Phi^{ASR,\infty}$ the maximal volume of ASR-phases and $A_{LAT}$ the advancement threshold below which the phases do not induce expansion. This threshold is a fitting parameter which should find its physical origin in the nature of the reactive aggregate and the cement paste properties. All the parameters delaying expansion lead to increases in the advancement threshold.

### 2.1.3. Internal pressure due to ASR

In the poromechanics framework, the action of ASR can be represented by the internal pressure, $P_{ASR}$, which acts in the porosity of the concrete and is evaluated from the volume of effective gel, $\Phi_{ASR}^{eff}$ :

$$P_{ASR} = M_{ASR} \cdot \langle \Phi_{ASR}^{eff} - \langle \Phi_{ASR}^{v,eff} + \Phi_{ASR}^{\Delta\phi} + \Phi_{ASR}^{pl} \rangle^{+} \rangle^{+} \qquad (4)$$

In Equation (4), the term $\Phi_{ASR}^{v,eff}$ represents the volumetric proportion of ASR products that can penetrate into the available porosity around the reactive sites according to the pressure. This dependence of the pressure on available porosity is necessary to model expansion under triaxial stresses [7]. This term corresponds to the proportion of ASR products by volume in the available porosity; it can increase with the pressure as explained in [7].

However, unrealistic responses appeared when the pressure of ASR products on the concrete decreases. External loading (or unloading after compression) can lead to a positive strain resulting in an increase in concrete porosity by deformation of the surrounding cement matrix and, thus, in a decrease of the pressure. As the volumetric proportion of ASR-products in the available porosity, $\Phi_{ASR}^{eff}$, was proportional to the internal pressure, the pressure decrease induced by the decompression of concrete led to the return of gel to its initial reactive site, slowing down the pressure decrease (which then kept a value high enough to provoke new cracks when the external compression stress was removed).

Such a phenomenon is not realistic because the ASR products partially crystallize (particularly in cement paste in presence of calcium ions [3]) and cannot return to the reactive site once formed. Therefore, the model was modified. In the present version, the modelling assumes that, once formed in aggregate or concrete porosity, the ASR-products can no longer move: the volume of ASR-products in the available porosity stays in the porosity even if the pressure decreases. Thus, $\Phi_{ASR}^{v,eff}$ is calculated using the maximum value of the ASR pressure found during the whole life of the structure, $P_{ASR}^{MAX}$ , instead of the current value of $P_{ASR}$:

$$\Phi_{ASR}^{v,eff} = \Phi_{ASR}^{v} \cdot \frac{P_{ASR}^{MAX}}{R_t} \tag{5}$$

This assumption is a simplification. The real behaviour is probably a combination of two phenomena: the part of a product that is not yet crystallized can probably still move in the porosity while the crystallized part is fixed. To illustrate this new particularity of the model, the initial and current hypotheses are both presented in Figure 2.

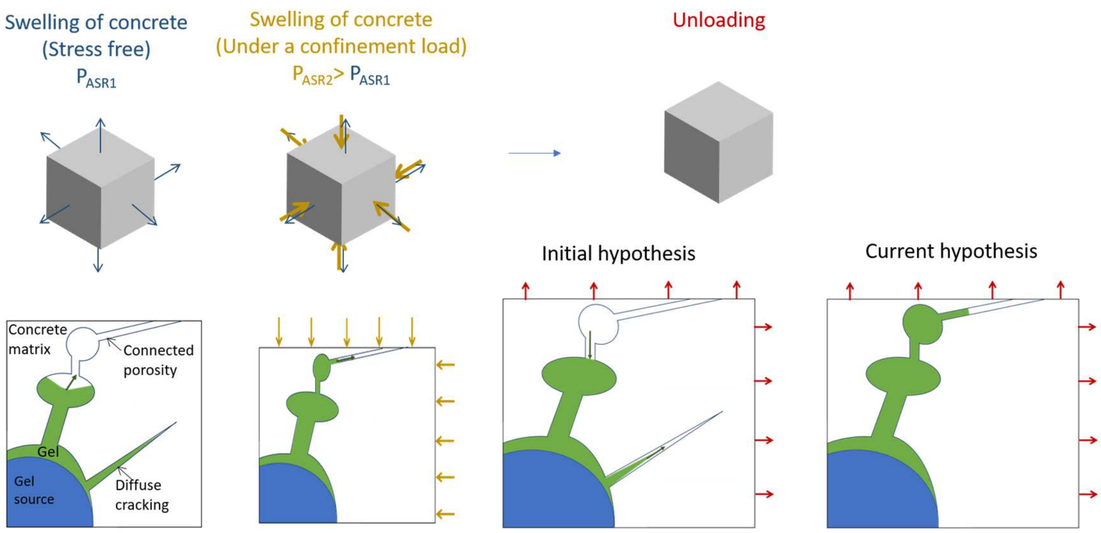


*Figure 1: Evolution of ASR gel in connected porosity in a stress-free state compared to a load/unload state; initial and current model hypotheses*

As volume strain causes the volume of porosity to vary, if the volume strain is positive, the pressure of ASR phases decreases (and conversely, the pressure increases if the volume strain is negative). The term $\Phi_{ASR}^{\Delta\phi}$of Equation (4) represents the variation of the porosity volume with volume strain, whatever the strain origin (elastic response of the material $\varepsilon^{el}$ or delayed response due to creep $\varepsilon^{cr}$).

$$\Phi_{ASR}^{\Delta\phi} = b_{ASR} \cdot tr(\varepsilon^{el} + \varepsilon^{cr}) \tag{6}$$

For the sake of simplicity and because of a lack of precise quantitative data on the filling of cracking induced by ASR, the model assumes the total filling of diffuse cracking, $\varepsilon^{pl,ASR}$, by ASR phases (term $\Phi_{ASR}^{pl}$ of Equation (4)). In the approach presented in the present paper, the diffuse cracking due to ASR is modelled by plastic strain, so this term is written as:

$$\Phi_{ASR}^{pl} = tr(\varepsilon^{pl,ASR}) \tag{7}$$

In Equation (4) and Equation (6), $M_{ASR}$ and $b_{ASR}$ are respectively the Biot modulus and the Biot coefficient related to ASR in concrete. They quantify the mechanical impact of the interactions between the different phases (ASR phases / aggregate and concrete) according to their respective rigidities.

The Biot coefficient is evaluated according to the effective volume of gel $\Phi_{ASR}^{eff}$ by a homogenization method [29]:

$$b_{ASR} = \frac{2\Phi_{ASR}^{eff}}{1 + \Phi_{ASR}^{eff}} \tag{8}$$

The Biot modulus is then assessed from $b_{ASR}$ and from the volume stiffness of the concrete matrix, $K_s$ , and of ASR products, $K_{ASR}$, according to the Biot theory [20,21]:

$$\frac{1}{M_{ASR}} = \frac{b_{ASR} - \Phi_{ASR}^{eff}}{K_s} + \frac{\Phi_{ASR}^{eff}}{K_{ASR}} \tag{9}$$

#### 2.1.4. ASR-diffuse cracking

##### *2.1.4.1. Criteria*

When the internal pressure induced by ASR exceeds the local effective tensile strength, $\widetilde{R_I^t}$ , ASR diffuse cracking is initiated. To drive this mechanism, an anisotropic associated Rankine criterion written in poromechanical terms is used:

$$f_I^{ASR} = \tilde{\sigma}_I{}^{eq} - \widetilde{R_I^t} \quad with \quad I \in [I, II, III]$$
$$and \quad \tilde{\sigma}_I{}^{eq} = P_{ASR} + \min(\tilde{\sigma}_I, 0) \tag{10}$$

where $\tilde{\sigma}_I$ is the stress in the principal direction I.

Once cracking is initiated, the crack opening is represented by the plastic strain, $\varepsilon_I^{pl,ASR}$ , and an increasing pressure is needed to propagate cracking. To represent this requirement, the tensile strength used in Equation (10) increases according to a linear hardening law. ~~The hardening law has been calibrated in previous numerical works~~ [30] ~~based on experimental results [4]~~. The hardening was close to 3% of the concrete Young's modulus. This small hardening is needed to provoke stable propagation of cracking. If its value tends to zero it is no longer possible to control the isotropy of free swelling because the cracking could appear arbitrarily in any principal direction and propagate to limit the rise of pressure in the gel, which, in turn, would be unable to initiate cracking in the other principal directions.

If a direction of the swelling concrete is reinforced [31] [8] [32] [33] [19], a chemical prestressing phenomenon occurs and leads to a small expansion along the reinforcement direction (the decrease of swelling amplitude in this direction is greater than the elastic effect of the steel bar alone [31]) and to a compressive stress (Figure 3-a and b). If the expansion is decreased in one direction (due to compressive stress), the effect of pressure in the model leads to greater expansion in the free directions, as observed for loaded specimens with a stress-free direction [26] [34] [35] [5] (Figure 3-a). The damage is smaller in the reinforced direction than for the stress-free specimen but is slightly greater in the direction perpendicular to reinforcement, due to the pressure rise induced by the hardening law (Figure 3-c).

The strain anisotropy is a consequence of stress state induced by reinforcement, and the anisotropy of stress state on swelling. The hardening law which manages this report phenomenon has been calibrated in previous numerical works [30] based on experimental results from [4].

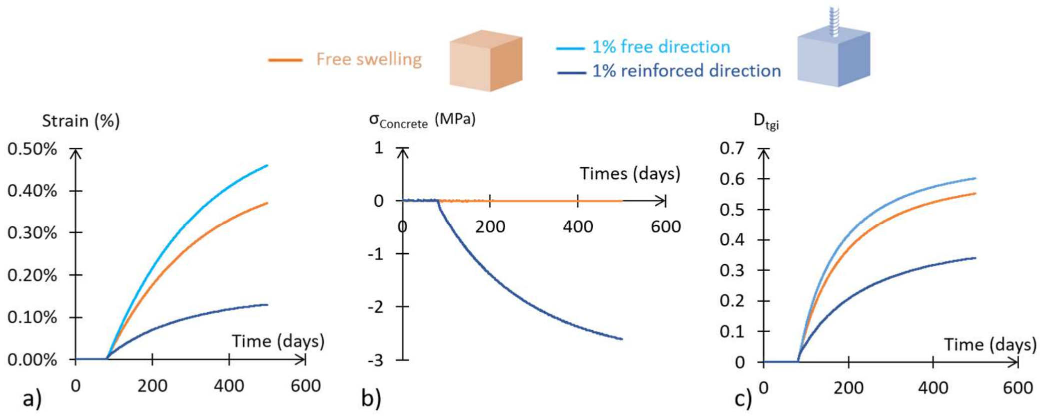


*Figure 2: Effect of reinforcement compared to stress-free swelling, a) Strain evolution, b) Concrete stress evolution, c) ASR-damage evolution*

### 2.1.4.2. Evolution of mechanical properties with ASR

As far as the mechanical strength degradation is concerned, the reduction of tensile strength and modulus is usually observed in most experimental studies [36] [37] [4] [38] [39]. The impact on the compressive strength is smaller and is more dependent on the concrete composition and test conditions [36] [40] [38] [5] [39] [37] [41].

In the present model, the damage induced by the swelling is anisotropic and assessed from the plastic strain obtained by the previous ASR-cracking criterion:

$$D_I^{t,ASR} = \frac{\varepsilon_I^{pl,ASR}}{\varepsilon_I^{pl,ASR} + \varepsilon^{k,ASR}} \tag{11}$$

where $\varepsilon^{k,ASR}$ is a characteristic strain evaluated at about 0.3% for the ASR [42].

The damage in compression is smaller, especially because of crack reclosure. It is evaluated from the combination of the tensile damage in the two orthogonal directions (Equation (12)). (See [43] [44] for further explanations on the concept and on its applicability to the ASR phenomenon.)

$$D_I^{c,ASR} = 1 - \left(\left(1 - D_{II}^{t,ASR}\right)\left(1 - D_{III}^{t,ASR}\right)\right)^{\alpha_{ASR}} \qquad with\ \ \alpha_{ASR} = 0.15 \tag{12}$$

The mechanical part of the model can also take the mechanism of swelling induced by the delayed ettringite formation (DEF) into account. Although the evaluation of the chemical advancement may differ, the mechanical consequences of induced pressure are close [45] and, thus, can be driven by the same equations [29]. Moreover, the mechanical part of the model has been validated in the ASR and DEF-context by the work of Morenon on laboratory reinforced beams with meshed reinforcement bars and non-reinforced dams [46]. The present study focuses on the interest of homogenized reinforced concrete in the context of ASR.

## 2.2. Concrete

It is important to note the difference between diffuse and structural cracking. Structural cracking can be induced by external loading, or by a strong strain gradient. Unlike cracks induced by ASR, structural cracks are localized. Different plastic criteria manage tensile and shear cracking. As this cracking occurs at the structural scale, their characterizations do not need the poromechanical framework. Thus, structural criteria are written in terms of total stresses instead of the poromechanical effective stress. By using these different kinds of criteria, the two type of cracking evolve independently. Finally, the total concrete stress $\sigma_{ij}^{c}$ is assessed by the combination of the diffuse and the structural cracking as in:

$$\sigma_{ij}^{c} = (1 - D_{ASR})(1 - D_{structural})\widetilde{\sigma_{ij}^{c}}$$

$$\widetilde{\sigma_{ij}^{c}} = \widetilde{\sigma_{ij}^{c}}' - \delta_{ij}(b_{ASR}P_{ASR}) \qquad (13)$$

The ASR damage, Biot coefficient and pressure have been already explained in Equations (11)-(12), Equation (8) and Equation (4) respectively. $\delta_{ij}$ is the Kronecker delta symbol, which is equal to one if i=j and zero otherwise. The evaluation of structural damage is presented in the following lines.

In tension, pre-peak and post-peak damage are considered. The first is isotropic, and evaluated from the mechanical characteristics of the concrete: its Young's modulus, E, its tensile strength, $R_t$, and the value of strain at the tensile peak $\varepsilon_{pic}^{t}$ (Equation (14)).

$$D_{pre-peak}^{t} = 1 - \frac{R_t}{E\varepsilon_{pic}^{t}} \tag{14}$$

After the peak, if loading is anisotropic, damage becomes anisotropic too. Structural cracking is then managed by a combination of plasticity and damage theories. Plastic strains are assessed through an anisotropic associated Rankine criterion (15). If pre-peak tensile damage exists, it is taken into consideration through a reduction of the tensile strength used in the following equations:

$$f_I^t = \tilde{\sigma}_I - \widetilde{R_I^t} \;\; with \;\; I \in [I, II, III]$$

$$\text{With } \widetilde{R_I^t} = \frac{R_t}{1 - D_{pre-peak}^{t}} \tag{15}$$

The anisotropic induced damage is:

$$D_I^t = 1 - \left(\frac{w_I^{k,t}}{w_I^{k,t} + w_I^{pl,t,max}}\right)^2 \tag{16}$$

where $w_I^{k,t}$ is the characteristic crack opening corresponding to the fracture tensile energy $G_{ft}$ and $w_I^{pl,t,max}$ is the maximal crack opening obtained with the value of plastic strain and element size in the principal tensile direction.

To be independent of the mesh size, an energy regularization based on the Hillerborg method is used. The approach consists of using the maximal distance between two nodes of the finite element in the considered direction as the dissipation length (details can be found in [47]).

The model can also consider structural damage in shear and compression, and even damage induced by crack reclosure. These parts of the model are not described here but can be found in [16]. To illustrate these behaviour laws, an example of a uniaxial cyclic load is given in Figure 4.

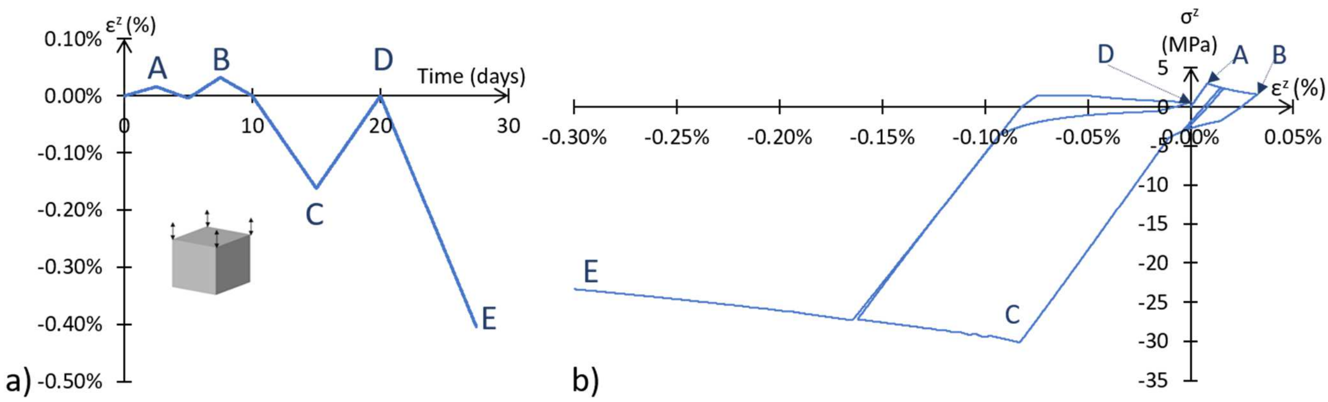


*Figure 4 : Uniaxial-tension-compression loads with damage, (Rt=3MPa, Rc=30MPa), a) Imposed strain versus time, b) Model response*

## 2.3. Reinforcement

The aim of the homogenized approach is to avoid explicit meshing of the reinforcement. The material is directly a 'reinforced concrete' without distinction between rebars and concrete in the mesh. Several directions of reinforcements can be considered in each finite element. Each steel rebar is defined by its direction (a vector field) and its surface ratio $\rho^r$ (a scalar field expressed as the ratio between steel and concrete cross-sections). The mechanical properties of the reinforcement (Young's modulus $E^r$, limit of elasticity $f_y^r$ , hardening coefficient $H^r$) form the input data.

The mechanical behaviour of the reinforcement is driven by an elastoplastic law controlled by a kinematic uniaxial plastic hardening criterion (17):

$$f^r = \left|\sigma^r - H^r \varepsilon^{r,pl}\right| - f_y^r$$

$$\textit{with}\ \ \sigma^r = E^r(\varepsilon^r - \varepsilon^{r,pl}) \tag{17}$$

## 2.4. Combination of concrete and reinforcement

The stress in homogenized reinforced concrete, $\sigma_{ij}$, is the combination of the stress in the concrete, $\sigma_{ij}^{c}$ (assessed by Equation 13), and that in the reinforcement, $\sigma_{ij}^{r,n}$ according to the steel/concrete ratio, $\rho^{r,n}$:

$$\sigma_{ij} = \left(1 - \sum_{n=1}^{Nr} \rho^{r,n}\right) \sigma_{ij}^{c} + \sum_{n=1}^{Nr} \rho^{r,n} \sigma_{ij}^{r,n} \qquad (18)$$

with $Nr$ the number of types of reinforcements. As in the previous part, an example of a uniaxial cyclic load is given to illustrate this behaviour law in Figure 5.

Homogenized reinforced concrete based on this approach has already been used for the evaluation of a nuclear power plant containment wall without ASR [48].

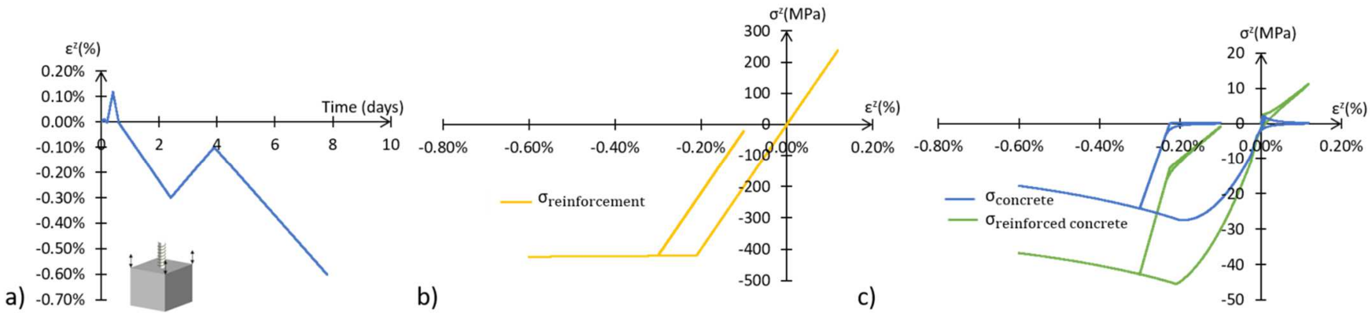


*Figure 5 ; Uniaxial-tension-compression loads with damage, (Rt=3MPa, Rc=30MPa), a) Imposed strain versus time, b) Reinforcement stress, c) Concrete and reinforced concrete stress*

# 3. Study case

## 3.1. Details of the experiments used for the validation [19]

The model is now used to reproduce the results obtained in the experimental study performed by Ohno et al. [19] on the structural behaviour of reinforced concrete beams affected by ASR. To consider different levels of ASR degradation, the beams were tested to failure after two ageing phases, of 17 and 45 months. Four beams were monitored: two reactive and two non-reactive beams. After the ageing period under natural weather, the beams were loaded to failure by a four-point bending test.

Transversal reinforcement was ensured by 10 mm diameter bars, and longitudinal reinforcement by 4 x 25 mm diameter bars. The location of the reinforcement is shown in Figure 6.

| Reinforcement | | |
|---|---|---|
| $fy_{HA25}$ | 420 Mpa | |
| $fy_{HA10}$ | 399 MPa | |
| E | 200 GPa | |
| H | 1.0 GPa | |
| **Concrete** | | |
| E | 37 GPa | |
| Rc | 27.5 MPa | |
| Rt | 2.2 MPa | (NF_EN_1992) |

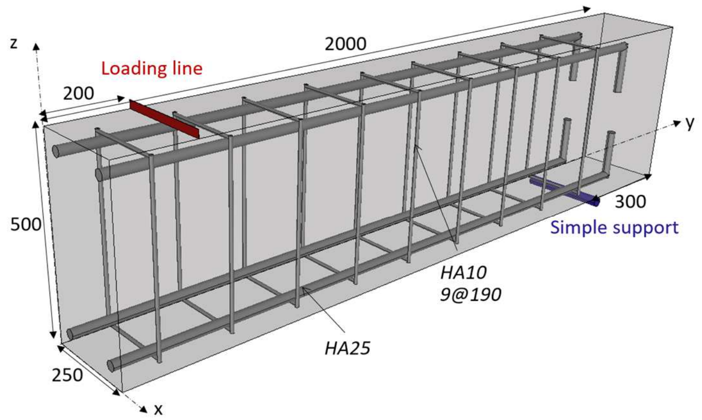


*Figure 3 : Mechanical characteristics and half-beam reinforcement (unit = mm)*

The compressive strength and Young's modulus of the two concretes (sound and reactive) used for the simulation of the beams were supplied by the authors of the experimental programme. The concrete properties used in the numerical evaluation are given in Figure 6. They are representative of concrete after long cement hydration without ASR damage (properties of the non-reactive concrete at 17 months). For simplicity, the gain of mechanical properties by hydration, which can partly counteract ASR damage [49], is not computed in this study and the impact of ASR on mechanical properties is directly evaluated by the model during expansion (see part 2.1.4.2). Due to the difference between material types (mortar or concrete), the mechanical properties and the value of mechanical parameter (Rt, Rc, E, $G_{ft}$ …) can be different. Hence, these differences are directly considered by the input data of the model.

## 3.2. Mesh used in the numerical analysis

In order to validate the ability of the model to treat large finite elements with the homogenized behaviour law of reinforced concrete affected by ASR, the numerical study uses three mesh sizes: M0 is the finest mesh and M2 the coarsest (Figure 7). The modelling was performed with 8 nodes cube elements with linear interpolation functions.

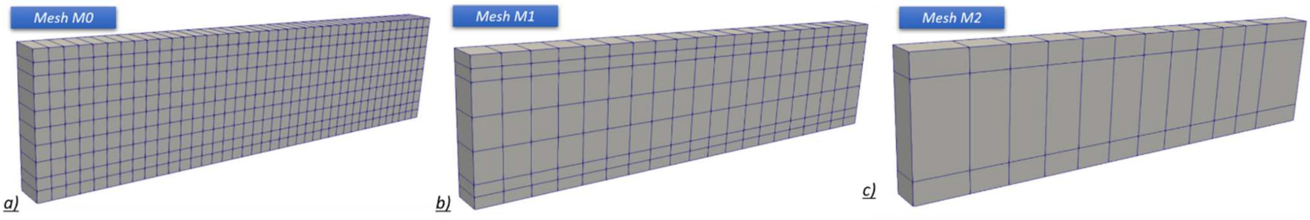


*Figure 7 : a) The finest mesh M0, b) The intermediate mesh M1, c) The coarsest mesh M2*

To obtain a realistic structural response in bending, homogenized finite elements were designed to respect the real positions of reinforcements barycentre. Figure 8 presents the mesh M0 with the ratios of homogenized reinforcements used in the three directions:

- the transversal and the longitudinal reinforcements are in the upper and lower parts of the beam, around the position of the centre of gravity of the longitudinal bars (Figure 8-a, b and c),
- To avoid making the mesh too sophisticated, vertical reinforcements are homogenized along the whole length of the beam (Figure 8-d).

In the model, the reinforcement ratio is obtained by dividing the area of the steel reinforcement by the cross-section of the area of the homogenized reinforced concrete (red area in Figure 8).

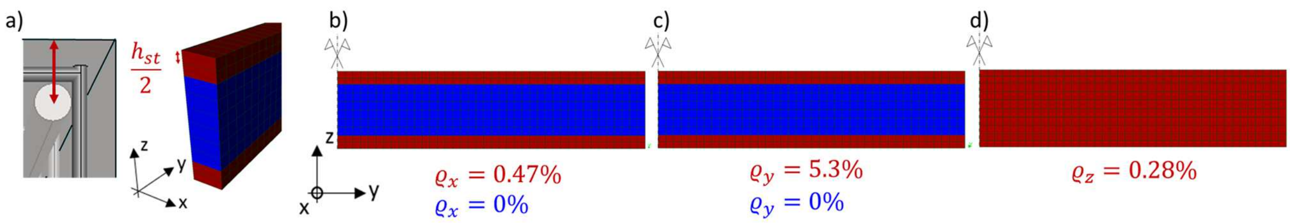


*Figure 4 : a) Height of reinforced area, b) Transversal reinforcement, c) Longitudinal reinforcement, d) Vertical reinforcement (red areas are homogenized reinforced concrete, blue areas are concrete without any reinforcement)*

Since the geometry is symmetrical, only a quarter of the beam is meshed. To ensure the induced symmetry conditions, axial displacements are blocked on the longitudinal and transversal internal faces. The displacements are blocked vertically on a line (linear simple support), and a loading line is also defined for the final loading to failure of the beam (Figure 9).

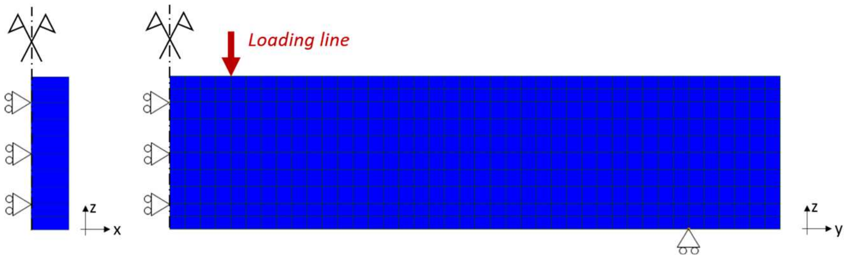


*Figure 5 : Boundary conditions*

# 4. Numerical results

## 4.1. Ageing phase

### 4.1.1. Structural response of the modelling

The ageing period is simulated first. During this phase, the beams were exposed to natural weather [19]. The seasonal variation of temperature imposed on the beams is given in Figure 10. Note that these values were provided by the nearest meteorological station. Hence, they may not correspond exactly to those of the experimental site and, as the region where the beams were stored is relatively wet, an environment with a constant relative humidity of 90% was assumed for the concrete.

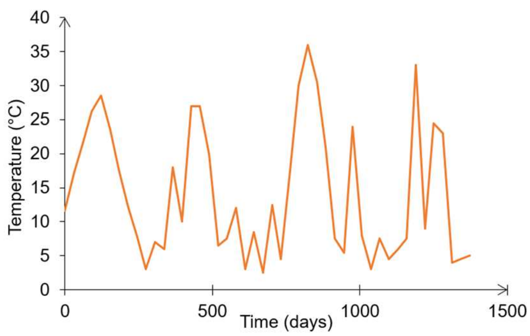


*Figure 6 : Set temperature*

Realistic temperatures are used in the numerical simulation to be representative of the real environmental conditions. Because ASR is activated by the temperature, it is particularly important to reproduce rapid and slow swelling rates due to low and high temperatures (Figure 10).

The vertical and longitudinal strains were monitored on the real reactive and non-reactive beams [19]. To measure the strains, the authors used six monitoring points along the longitudinal direction, and eight points for the vertical directions, distributed along the whole length. The basis of measurement was 100 mm and 300 mm for the longitudinal and the vertical directions, respectively. For the modelling, the points used to evaluate the strains are shown by blue and yellow arrows in Figure 11-a.

Although some small variations are visible between numerical and experimental strains, the global evolutions of longitudinal and vertical strains are well simulated by the model (Figure 11-b and Figure 11-c).

The strain of the non-reactive beams is reproduced through a usual dilation coefficient of $1.10^{-5}$ m/°C. The small differences between numerical and experimental data for non-reactive beams can be explained by the temperature difference between the laboratory and the meteorological station where temperatures were measured. However, the amplitude of most of the seasonal changes in temperatures are well reproduced.

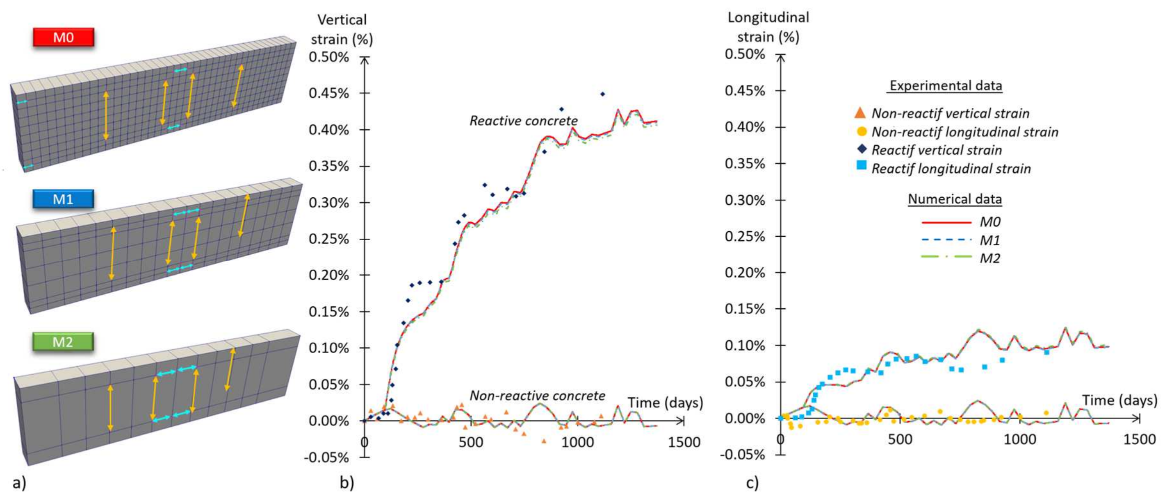


*Figure 7 : a) Monitoring points, b) Vertical strain, c) Longitudinal strain*

The anisotropic expansions of the reactive beams are also correctly simulated. They are obtained by the parameters given in Table 1. The small longitudinal strain induced by the effect of reinforcement on ASR expansion is well-evaluated. It is obtained with the hardening law used to evaluate the pressure due to ASR phases in the reactive concrete (Equation (10)). The law was not modified in the present work. The calculations used the calibration performed by Morenon et al. in [30] directly, throughout the analysis of samples damaged by ASR in laboratory conditions [34]. The interest of the law is that it depends on two usual mechanical properties of concrete (the modulus and the tensile strength). This leads to robust modelling with no need for new calibration to simulate the behaviour of different concretes. In addition, the amplitude of the vertical strain is correctly evaluated and a slight overestimation of the longitudinal strain can be observed, thus confirming the capability of the ASR-modelling to reproduce anisotropic expansion in field conditions.

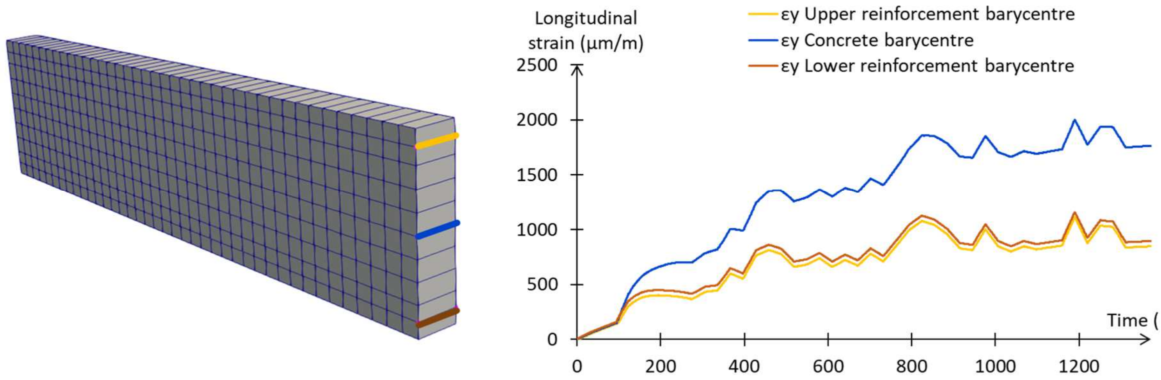


*Figure 8 : Strain evolution between the reinforcements and concrete barycentre*

To highlight the restraining effect, the differences in longitudinal strains between reinforcement and concrete can be observed at their barycentre. Strains are raised on nodes on both sides of the beam, averaged according to their height and presented in Figure 12. At the end of the ageing phase and with this configuration, the limitation of swelling in the reinforced part is up to 50% compared to the part without reinforcement. Besides, due to additional Poisson effect induced by the gravity, the lower reinforcement strain is slightly higher than the upper strain (about 50 µm).

| Parameter | Symbol | Corresponding | Value |
|---|---|---|---|

| | | equation | |
|---|---|---|---|
| Total gel production | $\phi^{ASR,\infty}$ | (3) | 7% |
| Void accessible by gel under a pressure equal to Rt | $\phi_{ASR}^{v}$ | (5) | 1.26% |
| Characteristic time of the reaction | $\tau_{ref}^{ASR}$ | (1) | 60 days |
| Advancement of the reaction at the beginning of observable swelling | $A_{LAT}$ | (3) | 0.05 |

*Table 1 : ASR input parameter values*

The model of homogenized reinforced concrete gives correct anisotropy of the measured expansion. The absence of specific meshing of the reinforcement bar does not cause any problem when the global deformation of structures damaged by ASR during their service lives is evaluated.

At the end of the period, the modelling predicts a mean chemical prestressing of about 2.6 MPa in the concrete cross-section of the reactive beams after 17 months and 3.3 MPa after 45 months. This is in good agreement with the chemical prestressing evaluated during the experimental programme [19].

The model is able to evaluate the diffuse and anisotropic ASR damage (Equation (6)). The first part of Figure 13 presents the damage fields according to the three principal directions for the 45 month reactive case modelled with the finest mesh. Figure 13-b shows a scheme of cracks induced by the ASR expansion obtained at the end of the ageing period. Diffuse cracking is visible along vertical and horizontal directions. As the reinforcement quantity is highest in the longitudinal direction, the chemical prestress is greatest in this direction. Hence, the damage is lowest in the longitudinal direction and the transfer of expansion induces greater damage in the ~~vertical and transversal~~ others directions. This is consistent with the experimental scheme. Nevertheless, the scheme was not sufficiently precise to obtain quantitative comparison.

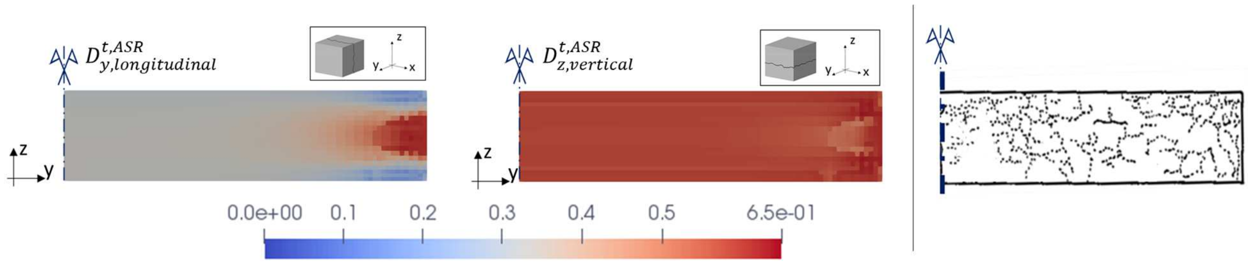


*Figure 9 : Anisotropic swelling damage for the 45 month case*

### 4.1.2. Sensitivity to the mesh

Three finenesses of mesh were used. All the results for the ageing period are presented in Figure 11. The differences in strain are very small between the solutions obtained for the different mesh densities (around $10^{-6}$ for the non-reactive beam and around $10^{-5}$ for the reactive one). ASR leads to highly intertwined calculations between chemical advancement, damage and creep and hence to numerous approximations. It represents relative scattering of less than 1.5% for the longitudinal and vertical maximal strain amplitude, and it remains correct whatever the mesh size.

The differences in mesh density induce small variations in chemical prestress. Between the finest and the coarsest mesh, a maximum scattering of 1.5% is reached. The difference between the finest and the intermediate mesh is smaller than 0.5%. For the non-reactive beams, the stress is very small with no significant variations according to mesh density.

The parametric study highlights the small dependence of the modelling of homogenized reinforced concrete on mesh density during ageing due to ASR. Coarse mesh can give a reliable evaluation of the service life of reinforced structures affected by ASR and thus reduce computational time.

## 4.2. Bending test to failure

### 4.2.1. Structural analysis

#### *4.2.1.1. Load – Deflection curves*

Following the ageing phase, the bending test is simulated by the application of an imposed displacement on the loading line. The nodal forces on this line and the vertical displacement at mid-span are then obtained to establish the load-deflection curves (Figure 14).

The load-displacement curves given by the numerical simulations are in accordance with the experimental curves. The duration of the ageing period has no impact for the modelling of the non-reactive beams, as hydration is not taken into account (and leads to small differences for the experimental data). The differences between numerical results and experimental data are greater for the reactive beams, mainly in the intermediate part, after first concrete cracking and before steel yielding. In this stage, the model slightly overestimates the force taken up by the beam.

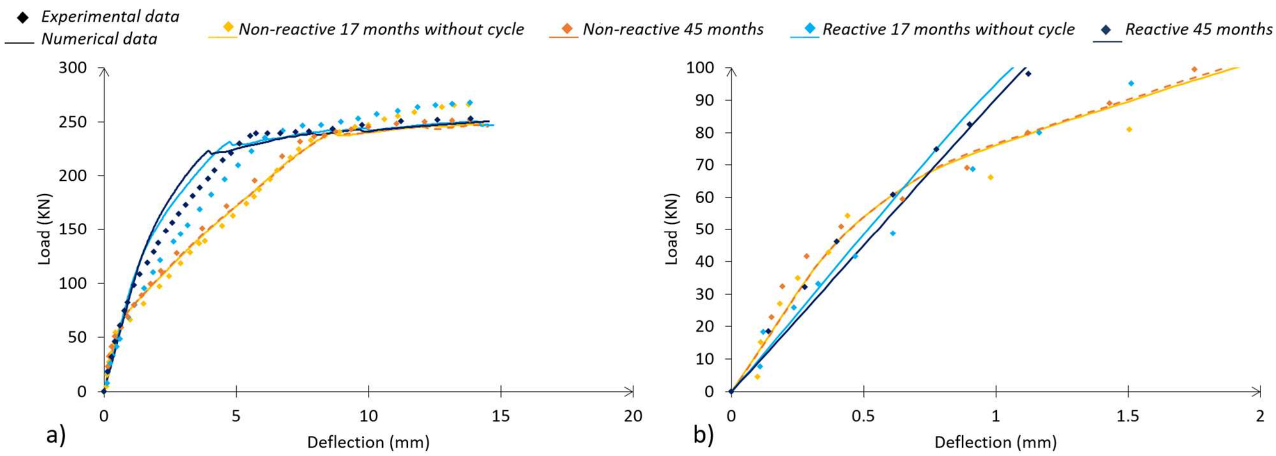


*Figure 10: M0 Direct load/deflection curves, a) Full evolution, b) Focus on the beginning*

The differences of behaviour between the reactive and non-reactive beams observed for the experiments are well reproduced:

- At the beginning of the loading, the reactive beam is slightly less rigid than the non-reactive one, due to the damage induced by ASR-expansion during the ageing-period (Figure 14-b)).

- After the first tensile crack in the lower part of the beam, the trend is inversed. The non-reactive beams present a rapid decrease of rigidity while the rigidity of the reactive beams remains unchanged. The conservation of rigidity for the reactive beams is due to the chemical prestressing induced by the ASR-expansion restrained by the reinforcement bars. It explains the delay of tensile cracking in the lower part.
- Steel yielding is obtained for the same loading for all the beams (the simulations reproduce yielding well). The deflection at yielding is lower for the reactive than for the non-reactive beams, both in experimental and numerical data. This reduction of elastic domain is due to the prestressing of reinforcements, which are already under tension before the start of the bending test for ASR concrete, due to the swelling occurring before the test.

In the second part, the impact of the chemical prestressing seems slightly too marked for the reactive beams. A parametrical study was performed in order to understand this overestimation, and pointed out the following issues:

- Evaluation of the rigidity of concrete subjected to ASR: in order to limit the number of parameters and because of missing data, the model uses some calibrated values (fracture energy and creep velocity, for instance). In fact, because of their relation to the nature of the gel and its impact on the matrix, a particular test is needed to establish a quantification process for some mechanical parameters:
    - Damage of reactive concrete is calculated through $\varepsilon^{k,ASR}$. This parameter has already been calibrated on previous works [42]. It drives the impact of ASR damage according to the value of ASR plastic strain on the concrete strength. Hence, a mechanical strength test is needed on reactive concrete after the ageing phase to calculate this value.
    - Evolution of ASR plastic strain is managed by a hardening law, also previously calibrated [30]. This ratio controls the rise of internal pressure during swelling. To estimate this law, confining tests could be done during the swelling phase.
- Availability of ASR-products for new expansion during flexural loading:

- The assumption on the location of ASR product in porosity has a strong impact on the response of the model to failure tests. With the assumption that the volume of ASR products is proportional to the pressure and able to create new expansion in case of unloading as performed in [7], the rigidity of reinforced beams would be greatly decreased for the beams studied in this paper (Figure 15) Consequently, this assumption has been modified: in the present work, it is assumed that ASR-products are totally blocked in the porosity and cannot lead to new expansion even in case of a decrease in the compressive stress (see the discussion in part 2.1.3). This new assumption seems to lead to too much rigidity (Figure 15) The best modelling could be obtained by combining the two mechanisms but, without clear experimental data or observations on this point, it is difficult to precisely evaluate the percentage of ASR products able to lead to new expansion during the flexural test.

- Steel-concrete interface ~~Concrete/steel bonding~~ after ASR-expansion in reinforced concrete:
    - During usual flexural tests on reinforced beams, the loss of bond generally starts and increases during this intermediate phase of the test. In the present work, the assumption of perfect bonding between concrete and steel used in the homogenized reinforced concrete modelling can lead to an overestimation that could be representative of the real tests. Sliding between concrete and steel could lead to larger flexural cracks and thus to a greater loss of rigidity than predicted by the model.

Future works will focus on this last aspect to improve the precision of the model in the reproducibility of the behaviour of reinforced structures damaged by ASR after flexural cracking.

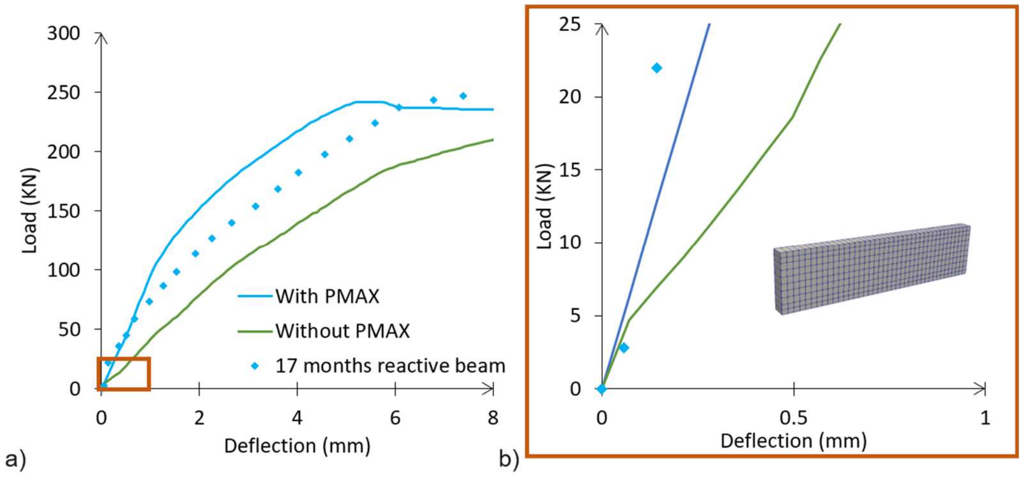


*Figure 11 : Evolution induced by the PMAX implementation a)Global evolution b)Focus on the beginning*

Small differences are induced by the ageing phase for the reactive beams from 17 to 45 months. ASR advancement is therefore slightly higher in the beam tested at 45 months. It induces greater damage in the beam and leads to the difference of rigidity observed in the simulations for loads higher than 150 KN. Even though the model slightly overestimates the impact of chemical prestress on beam rigidity, it is able to recover this ageing difference between reactive beams.

#### 4.2.1.2. Load – Deflection curves of cyclic loading

Beams tested after 17 months were subjected to a loading cycle before failure. The corresponding load displacement curves are presented in Figure 16. The difference between the two behaviours is well reproduced and observations are similar to previous results.

First, the figure shows the capacity of the damage modelling to reproduce the evolution of the rigidity of reinforced structures for usual concrete. Second, despite the slight overestimation of the bending force, the structural rigidity of the reactive beam is well-evaluated during the unloading. This confirms the correct evaluation of concrete rigidity during this phase. The reason for the overestimation of the force during loading has to be sought in other aspects of the model.

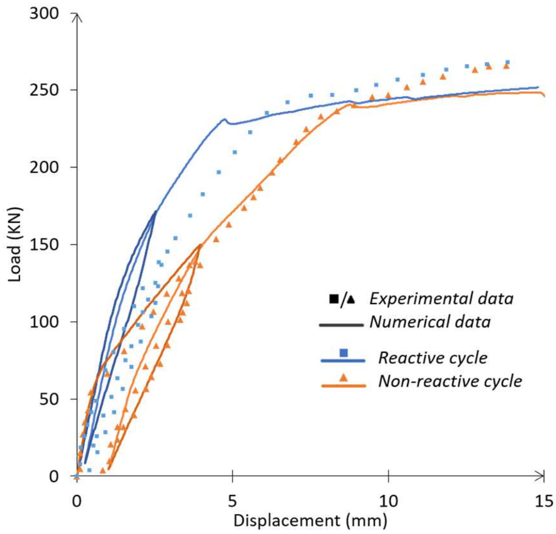


*Figure 12 : 17 month load-displacement curves with a cyclic load*

Finally, the present study confirms the conclusions drawn in [19] [4] [50]: ASR has only a slight impact on the flexural behaviour of the reinforced beam when beams are calculated for a failure due to steel yielding. No significant influence is observed on the ultimate bending behaviour but the evolution of the rigidity during the failure test is impacted by the compressive stress induced when the expansion is restrained by the reinforcement. Nevertheless, as seen previously in Figure 13, ASR induces non-negligible diffuse cracking on reactive beams. Due to these anisotropic micro-cracks, reactive beams show poorer durability than non-reactive ones.

### 4.2.2. Structural cracking

The structural cracking observed during the experimental programme is represented at the top of Figure 17.The comparison between reactive and non-reactive beams highlights the limited number of structural cracks due to the loading of the reactive beam. During experimental observations, about six structural cracks were noted on half of the non-reactive beam, versus only two main cracks for the reactive beam (top of Figure 17).

The structural crack patterns obtained by the modelling are presented at the bottom of Figure 17. The meshes show the maximal value of crack opening along the beams. The number, location, and direction of cracks are correctly reproduced by the model (with five major cracks for the non-reactive beam and only one for the reactive beam at 45 months). The difference between reactive and non-reactive beams in terms of limitation of number of structural cracks for beams with ASR is thus reproduced by the model. The difference can be explained by the chemical prestressing of reactive beams. The compressive stress induced when the expansion is restrained by the reinforcement prevents the opening of the shear cracks close to the supports for the reactive beams. For this reason, the non-reactive beam shows almost three shear cracks while the 17 month reactive beam has only two thin shear cracks and the 45 month reactive beam has only one, very thin, shear crack. In addition, the younger reactive beam shows slightly greater crack opening than the 45 month beam. This difference can be explained by the slight difference in chemical prestressing and damage according to the duration of the ageing period.

The use of homogenized reinforced concrete leads to acceptable reproducibility of the crack pattern at the end of a bending test for both non-reactive beams and ASR-damaged beams and it is able to reproduce the difference between non-reactive and reactive beams.

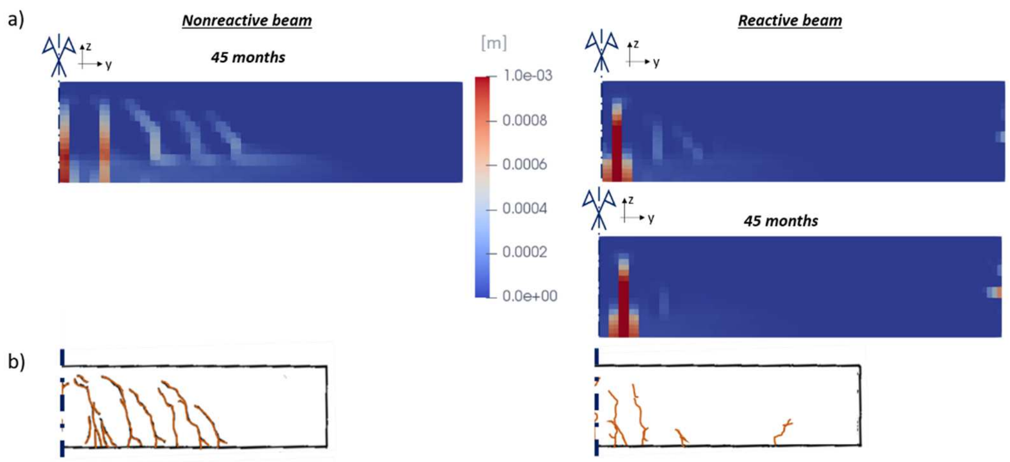


*Figure 17 Structural crack opening a)Crack pattern obtained by modelling, b) Scheme of real crack pattern from [19]*

### 4.2.3. Mesh sensitivity

The three densities of mesh are compared in Figure 18. The curves obtained for the non-reactive beams tested at 17 and 45 months are represented in Figure 18-a and b. The curves obtained for the ASR-reactive beams tested at 17 and 45 months are represented in Figure 18-c and d respectively.

For all the configurations, the flexural behaviour during the failure test shows negligible sensitivity to mesh size. Even the coarsest mesh - M2 with only 1 finite element in the height to represent the plain concrete between the two reinforced parts (top and bottom) - gives a correct prediction for the non-reactive beams. Only the rigidity of the cracked non-reactive beams is slightly underestimated for loads higher than 100 kN by the two coarsest meshes (M1 and M2). Concerning the curves of the reactive beam, the variation induced by mesh size is less visible than for the non-reactive beams, especially between M0 and M1. For both ageing periods, maximal variation is observable in the M2 mesh during the start of the yielding phase. The overestimation of rigidity above the force corresponding to the concrete cracking for the reactive beams is similar for all the meshes.

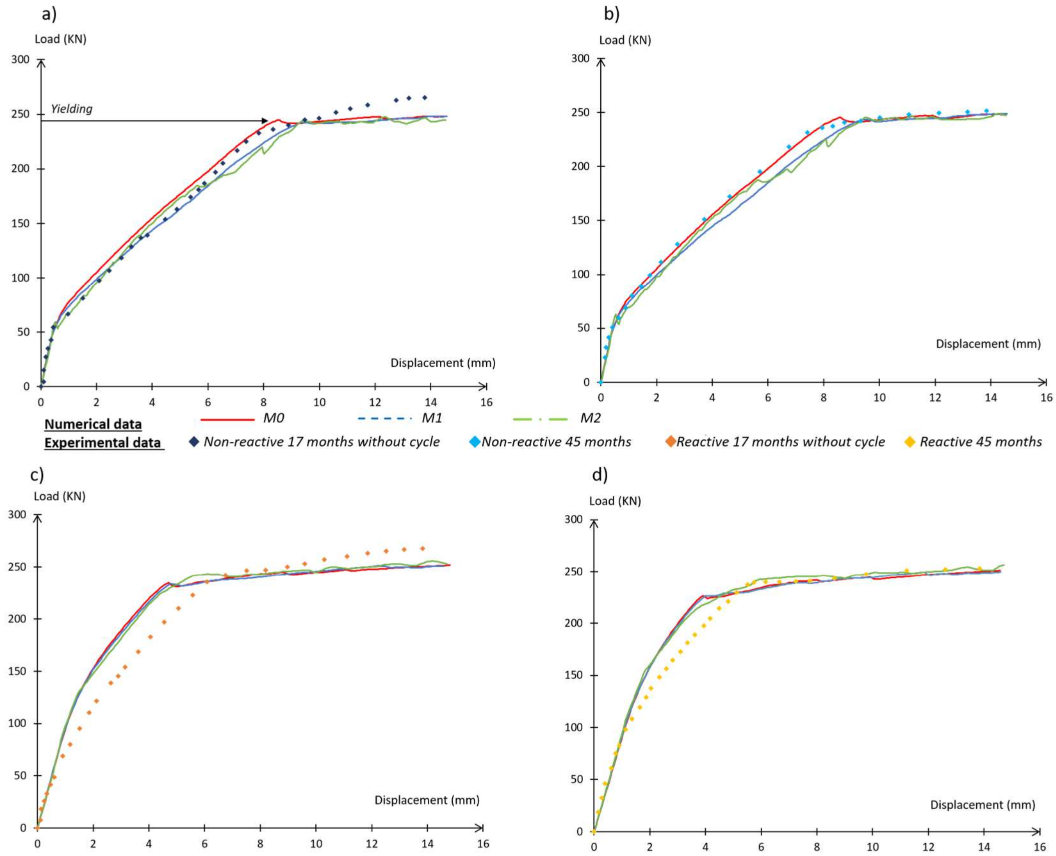


*Figure 13 Load-displacement curves a) Non-reactive beam after 17 months without cycle, b) Non-reactive beam after 45 months, c) Reactive beams after 17 months without cycle, d) Reactive beams after 45 months*

The low dispersion between these values highlights the independence of the model prediction towards the mesh as far as the structural behaviour is concerned, more specifically for the reactive beams.

Figure 19 shows the crack patterns obtained for the three meshes. The locations of the structural cracks are well-reproduced by the three meshes although there is a loss of crack locations for the mesh M2 due to the small number of elements in the length. In the non-reactive case, the flexural crack opening is almost twice as large with the coarsest mesh (M2) as with the finest mesh (M0), but only one crack appears for M2, versus two cracks for the finest mesh. This finally leads to similar results in terms of 'cumulative crack opening' but with a less accurate location for the coarser mesh. The distance between the two cracks observed with the mesh M0 is small compared to the size of the elements used in the meshes M1 and M2. These meshes cannot differentiate between two cracks in this zone with the element sizes used.

The number of cracks in a homogenized element subjected to tension is defined according to the bond conditions (anchorage length, bond strength) and the fracture energy [13]. The shear cracks at the end of the failure test are well-reproduced for the non-reactive beam with the mesh M0 and, even though the modelling is less accurate with the two coarsest meshes, M1 and M2, these cracks are nevertheless considered by the tensile damage occurring in this zone.

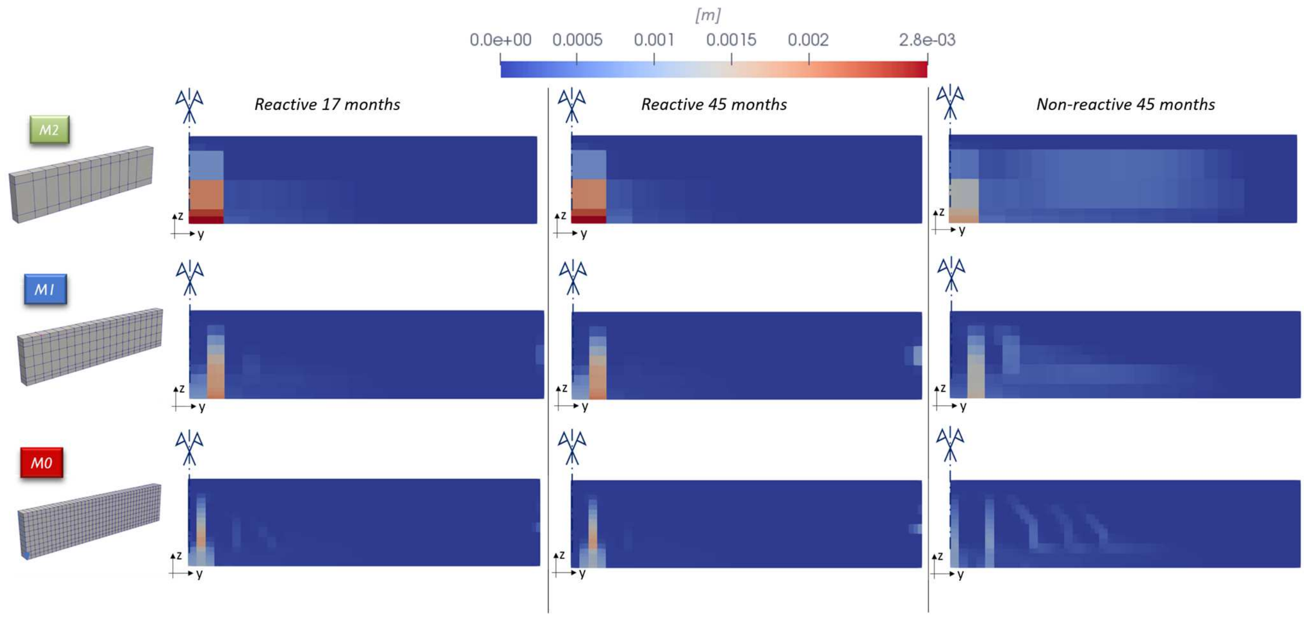


*Figure 14 Structural crack opening for all the meshes*

## 5. Conclusion

The aim of the present paper was firstly to evaluate the capability of a homogenized reinforced concrete model to reproduce the behaviour of beams damaged by ASR during the service life and by a failure bending test. Secondly, the stability of the response according to mesh size was estimated.

The results obtained for the ageing period show a correct distribution of anisotropic deformations with respect to the experimental results. They were obtained thanks to the anisotropic criteria and to the hardening law of the model developed in previous work. New calibration was not performed but a modification was introduced concerning the nature of the ASR gel, for which a crystallization hypothesis was proposed to explain the absence of new cracking during final loading after ageing induced by the erasure of the compressive stress present during swelling. Experimental results reproduced in this paper were taken from experimentation performed on ASR beams in natural weather conditions. The present work shows that the model elaborated from laboratory results is able to reproduce tests in natural conditions.

In this work, the need to explicitly mesh the reinforcement bars is avoided thanks to the use of homogenized reinforced concrete elements. This is of particular interest for large reinforced concrete structures, where the meshing of all rebars leads to computational costs incompatible with engineering processes.

The structural behaviours of the beams during the failure tests are correctly evaluated. Simulation using homogenized reinforced concrete is able to reproduce the load – displacement curves for all the beams. In particular, it predicts the positive impact of chemical prestressing on the behaviour of the beams subjected to failure tests, and its evolution over time. It can also reproduce the differences of structural cracking between reactive and non-reactive beams at the end of the bending test. For the reactive beams, the chemical prestressing induces a significant limitation of shear cracks, which is even more noticeable for a longer ageing period.

Numerical results obtained with the three meshes present small differences. The impact of element size on the calculations for this application is negligible but leads to a significant gain in computational time (which has to be balanced against a loss of precision in the location of cracks).

Although the differences between experimental and numerical data are limited, there is an overestimation on the load/displacement curves of the reactive beams in the intermediate phase after first concrete cracking and yielding. Various parametric studies have been performed to explain this fact. The assumption of gel crystallization, formulated to avoid gel returning to the reactive sites during final loading and causing decompression of the reactive concrete. While its consideration constitutes an improvement, it also could explain this slight overestimation of stiffness. An intermediate assumption could be to consider that some of the gel crystallizes and, in some, crystallization is delayed. However, this new assumption would require the introduction of a more complex chemical law able to consider ageing of ASR gel induced by an exchange of ions with the cement matrix. This could be a perspective for the continuation of this work.

Despite this slight transient overestimation of stiffness, the homogenized reinforced concrete approach in an ASR context is able to describe the significant effect of chemical pre-stress on the behaviour of reinforced structures, without explicit meshing of rebars. Its ability to quantify the crack opening could be used in the future to assess the evolution of the durability of ASR-damaged structures and the effects of its combination with other chemical disorders, such as carbonation and steel corrosion.

## 6. Acknowledgments

Dr S. Ohno and Dr Y. Kawabata are thanked for important detailed information on test conditions. The financial support of Electricité de France (EDF) for the EXIGENCE project, which is the framework of the present study, is acknowledged. The modelling was performed with the finite element software developed by EDF R&D, Code_Aster (V14.2, https://www.code-aster.org) and the post-processing with Salome_Meca.

## 7. References

[1] Glasser LSD, Kataoka N. The chemistry of ‘alkali-aggregate’ reaction. Cement and Concrete Research 1981;11. https://doi.org/10.1016/0008-8846(81)90003-X.

[2] Poole AB. Alkali-silica reactivity mechanisms of gel formation and expansion. Proceedings of the 9th International Conference on Alkali-Aggregate Reaction, London (England), vol. 104, Concrete Society Publications CS; 1992, p. 782–9.

[3] Ichikawa T, Miura M. Modified model of alkali-silica reaction. Cement and Concrete Research 2007;37. https://doi.org/10.1016/j.cemconres.2007.06.008.

[4] Multon S. Évaluation expérimentale et théorique des effets mécaniques de l’alcali-réaction sur des structures modèles. PhD Thesis. Université de Marne-la-Vallée, 2003.

[5] Gautam BP, Panesar DK. A new method of applying long-term multiaxial stresses in concrete specimens undergoing ASR, and their triaxial expansions. Materials and Structures 2016;49. https://doi.org/10.1617/s11527-015-0734-z.

[6] Liaudat J, Carol I, López CM, Saouma VE. ASR expansions in concrete under triaxial confinement. Cement and Concrete Composites 2018;86:160–70. https://doi.org/10.1016/j.cemconcomp.2017.10.010.

[7] Morenon P, Multon S, Sellier A, Grimal E, Hamon F, Bourdarot E. Impact of stresses and restraints on ASR expansion. Construction and Building Materials 2017;140:58–74. https://doi.org/10.1016/j.conbuildmat.2017.02.067.

[8] Jones AEK. Cracking, expansion and strength of concrete subjected to restrained alkali silica reaction. PhD Thesis. University of Birmingham, 1994.

[9] Kongshaug SS, Oseland O, Kanstad T, Hendriks MAN, Rodum E, Markeset G. Experimental investigation of ASR-affected concrete – The influence of uniaxial loading on the evolution of mechanical properties, expansion and damage indices. Construction and Building Materials 2020. https://doi.org/10.1016/j.conbuildmat.2020.118384.

[10] Hayes NW, Giorla AB, Trent W, Cong D, Pape YL, Ma ZJ. Effect of alkali-silica reaction on the fracture properties of confined concrete. Construction and Building Materials 2020;238. https://doi.org/10.1016/j.conbuildmat.2019.117641.

[11] Wiwat Puatatsananon and Victor Saouma. Chemo-Mechanical Micromodel for Alkali-Silica Reaction. ACI Materials Journal 2013;110. https://doi.org/10.14359/51684367.

[12] Wu T, Temizer İ, Wriggers P. Multiscale hydro-thermo-chemo-mechanical coupling: Application to alkali–silica reaction. Computational Materials Science 2014;84:381–95. https://doi.org/10.1016/j.commatsci.2013.12.029.

[13] Gallyamov ER, Cuba Ramos AI, Corrado M, Rezakhani R, Molinari J-F. Multi-scale modelling of concrete structures affected by alkali-silica reaction: Coupling the mesoscopic damage

evolution and the macroscopic concrete deterioration. International Journal of Solids and Structures 2020;207:262–78. https://doi.org/10.1016/j.ijsolstr.2020.10.010.

[14] Esposito R, Hendriks MAN. Literature review of modelling approaches for ASR in concrete: a new perspective. Null 2019;23:1311–31. https://doi.org/10.1080/19648189.2017.1347068.

[15] Li P, Tan N, An X, Maekawa K, Jiang Z. Restraint Effect of Reinforcing Bar on ASR Expansion and Deterioration Characteristic of the Bond Behavior. Journal of Advanced Concrete Technology 2020;18:192–210. https://doi.org/10.3151/jact.18.192.

[16] Sellier A. Anisotropic Damage and Visco-Elasto-Plasticity Applied to Multiphasic Materials. LMDC - Laboratoire Matériaux et Durabilité des Constructions de Toulouse ; Université de Toulouse III - Paul Sabatier ; INSA de Toulouse; 2018.

[17] Winnicki A, Pietruszczak S. On Mechanical Degradation of Reinforced Concrete Affected by Alkali-Silica Reaction. Journal of Engineering Mechanics 2008;134:611–27. https://doi.org/10.1061/(ASCE)0733-9399(2008)134:8(611).

[18] Sellier A, Millard A. A homogenized formulation to account for sliding of non-meshed reinforcements during the cracking of brittle matrix composites: Application to reinforced concrete. Engineering Fracture Mechanics 2019;213:182–96. https://doi.org/10.1016/j.engfracmech.2019.04.008.

[19] Ohno S, Yoshioka Y, Shinozaki Y, Morikawa T. The mechanical behaviour of reinforced beams coated after Alkali-Silica Reaction damage. 8th international conference on Alkali-aggregate reaction. Kyoto, Japan, 1989, p. 697–702.

[20] Biot MA. General theory of three-dimensional consolidation. Journal of Applied Physics 1941;12.

[21] Coussy O. Mécanique des milieux poreux. Editions Technip; 1991.

[22] KACHANOV LM. Time of the rupture process under creep conditions, Izy Akad. Nank SSR Otd Tech Nauk 1958;8.

[23] Weihe S, Kröplin B, Borst RD. Classification of smeared crack models based on material and structural properties. International Journal of Solids and Structures 1998;35:1289–308. https://doi.org/10.1016/S0020-7683(97)00104-2.

[24] Poyet S. Étude de la dégradation des ouvrages en béton atteints par la réaction alcali-silice : approche expérimentale et modélisation numérique multi-échelles des dégradations dans un environnement hydro-chemo-mécanique variable. PhD Thesis. Université de Marne-la-Vallée, 2003.

[25] POYET S, Sellier A, Capra B, Thèvenin-Foray G, Torrenti J-M, Tournier-Cognon H, et al. Influence of Water on Alkali-Silica Reaction: Experimental Study and Numerical Simulations. Journal of Materials in Civil Engineering 2006;18. https://doi.org/10.1061/(ASCE)0899-1561(2006)18:4(588).

[26] Larive C. Apports combinés de l'expérimentation et de la modelisation à la compréhension de l'alcali-reaction et de ses effets mécaniques. PhD Thesis. École nationale des ponts et chaussées (France), 1998.

[27] Bažant ZP, Steffens A. Mathematical model for kinetics of alkali–silica reaction in concrete. Cement and Concrete Research 2000;30:419–28. https://doi.org/10.1016/S0008-8846(99)00270-7.

[28] M. Idorn G. A discussion of the paper "Mathematical model for kinetics of alkali–silica reaction in concrete" by Zdenek P. Bazant and Alexander Steffens. Cement and Concrete Research 2001;31:1109–10. https://doi.org/10.1016/S0008-8846(01)00522-1.

[29] Sellier A, Multon S. Chemical modelling of Delayed Ettringite Formation for assessment of affected concrete structures. Cement and Concrete Research 2018;108:72–86. https://doi.org/10.1016/j.cemconres.2018.03.006.

[30] Morenon P, Multon S, Sellier A, Grimal E, Hamon F, Kolmayer P. Flexural performance of reinforced concrete beams damaged by Alkali-Silica Reaction. Cement and Concrete Composites 2019;104:103412. https://doi.org/10.1016/j.cemconcomp.2019.103412.

[31] Multon S, Seignol J-F, Toutlemonde F. Chemomechanical assessment of beams damaged by alkali-silica reaction. Journal of Materials in Civil Engineering 2006;18:500–9.

[32] Muranaka M, Tanaka Y. Development of Physical and Chemical Model for Concrete Expansion Due to Asr Based on Reaction Mechanism. Journal of Japan Society of Civil Engineers, Ser E2 (Materials and Concrete Structures) 2013;69:1–15. https://doi.org/10.2208/jscejmcs.69.1.

[33] Tsukada T, Koga H, Hayakawa T, Watanabe H, Kimura Y. Basic study about expansion and restriction of structural concrete deteriorated with alkali silica reaction. Proceedings of JSCE, vol. 276, 2010, p. 551–2.

[34] Multon S, Toutlemonde F. Effect of applied stresses on alkali–silica reaction-induced expansions. Cement and Concrete Research 2006;36:912–20. https://doi.org/10.1016/j.cemconres.2005.11.012.

[35] Berra M, Faggiani G, Mangialardi T, Paolini AE. Influence of stress restraint on the expansive behaviour of concrete affected by alkali-silica reaction. Cement and Concrete Research 2010;40:1403–9. https://doi.org/10.1016/j.cemconres.2010.05.002.

[36] Engineers I of S. Structural effects of alkali-silica reaction: Technical guidance on the appraisal of existing structures. Institution of structural engineers; 1992.

[37] Zhychkovska O. Effect of Alkali-silica Reaction (ASR) on Steel-concrete Bond. Thesis. 2020.

[38] Diab SH, Soliman AM, Nokken MR. Changes in mechanical properties and durability indices of concrete undergoing ASR expansion. Construction and Building Materials 2020;251:118951. https://doi.org/10.1016/j.conbuildmat.2020.118951.

[39] Esposito R, Hendriks MAN. Simulating the Deteriorating Effect of the Alkali-Silica Reaction in Concrete via a Micro-Poro Fracture Mechanical Model. CONCREEP 10, n.d., p. 118–27. https://doi.org/10.1061/9780784479346.015.

[40] Aryan H, Gencturk B, Hanifehzadeh M, Wei J. ASR Degradation and Expansion of Plain and Reinforced Concrete. Structures Congress 2020, American Society of Civil Engineers Reston, VA; 2020, p. 303–15.

[41] Giaccio G, Zerbino R, Ponce JM, Batic OR. Mechanical behavior of concretes damaged by alkali-silica reaction. Cement and Concrete Research 2008;38:993–1004. https://doi.org/10.1016/j.cemconres.2008.02.009.

[42] Capra B, Sellier A. Orthotropic modelling of alkali-aggregate reaction in concrete structures: numerical simulations. Mechanics of Materials 2003;35:817–30. https://doi.org/10.1016/S0167-6636(02)00209-0.

[43] Sellier A, Bary B. Coupled damage tensors and weakest link theory for the description of crack induced anisotropy in concrete. Engineering Fracture Mechanics 2002;69:1925–39. https://doi.org/10.1016/S0013-7944(02)00069-3.

[44] Sanchez LFM, Multon S, Sellier A, Cyr M, Fournier B, Jolin M. Comparative study of a chemo–mechanical modeling for alkali silica reaction (ASR) with experimental evidences. Construction and Building Materials 2014;72:301–15. https://doi.org/10.1016/j.conbuildmat.2014.09.007.

[45] Multon S, Sellier A. Expansion modelling based on cracking induced by the formation of new phases in concrete. International Journal of Solids and Structures 2019;160:293–306. https://doi.org/10.1016/j.ijsolstr.2018.11.001.

[46] Morenon P, Sellier A, MULTON S, Grimal E, Kolmayer P. ASSESSMENT OF A CONCRETE DAM AFFECTED BY AN INTERNAL SWELLING REACTION (ISR). NAFEMS, Paris: 2018.

[47] Morenon P. Modélisation des réactions de gonflement interne des bétons avec prise en compte des couplages poro-mécaniques et chimiques. PhD Thesis. Université Toulouse III-Paul Sabatier, 2017.

[48] Chhun P. Modélisation du comportement thermo-hydro-chemo-mécanique des enceintes de confinement nucléaire en béton armé-précontraint. PhD Thesis. Université de Toulouse, Université Toulouse III-Paul Sabatier, 2017.

[49] Pathirage M, Bousikhane F, D'Ambrosia M, Alnaggar M, Cusatis G. Effect of alkali silica reaction on the mechanical properties of aging mortar bars: Experiments and numerical modeling.

International Journal of Damage Mechanics 2019;28:291–322. https://doi.org/10.1177/1056789517750213.

[50] Bracci JM, Gardoni P, Trejo D. Performance of Lap Splices in Large-Scale Column Specimens Affected by ASR and/or DEF. Extension Phase, 2012.